

FERA: Foil Fencing Referee Assistant Using Pose-Based Multi-Label Move Recognition and Rule Reasoning

Ziwen Chen
 Marc Garneau Collegiate Institute (TDSB)
 Toronto, Canada
 ziwenc08@gmail.com

Zhong Wang
 Dalian University of Technology (DUT)
 Dalian, China
 zhongwang@dlut.edu.cn

Abstract

The sport of fencing, like many other sports, faces challenges in refereeing: subjective calls, human errors, bias, and limited availability in practice environments. We present FERA (Fencing Referee Assistant), a prototype AI referee for foil fencing which integrates pose-based multi-label action recognition and rule-based reasoning. FERA extracts 2D joint positions from video, normalizes them, computes a 101-dimensional kinematic feature set, and applies a Transformer for multi-label move and blade classification. To determine priority and scoring, FERA applies a distilled language model with encoded right-of-way rules, producing both a decision and an explanation for each exchange. With limited hand-labeled data, a 5-fold cross-validation achieves an average macro-F1 score of 0.549, outperforming multiple baselines, including a Temporal Convolutional Network (TCN), BiLSTM, and a vanilla Transformer. While not ready for deployment, these results demonstrate a promising path towards automated referee assistance in foil fencing and new opportunities for AI applications, such as coaching in the field of fencing.

1. Introduction

Refereeing plays a fundamental role in competitive sports, ensuring fairness and consistency. In fencing, the referee’s job is often more complex than in other sports: they must evaluate blade interactions, interpret right-of-way, and consider who initiated the attack, all at very high speed. Even at official competitions with trained referees, disputes and inconsistent calls still arise due to human error. In club settings, the problem is worse: bouts are often refereed by fellow members or proceed without a referee at all.

The task at hand, however, is more challenging than it first appears. AI refereeing requires robust recognition of temporally dependent actions under occlusion and high speed. Existing fencing action datasets are narrow in

scope, covering only a few footwork moves from individual fencers, often under fixed camera angles. As a result, they fail to generalize to real bouts involving two fencers, interactions, and diverse viewing conditions. To overcome this limitation, we created a new dataset and labeling protocol.

Together with this dataset, we introduce FERA (Fencing Referee Assistant), a four-stage pipeline that: (i) 2D pose extraction, (ii) kinematic and temporal feature computation, (iii) a Transformer encoder for multi-label move and blade classification (FERA-MDT), and (iv) a distilled language model that applies encoded right-of-way rules for final decisions (FERA-LM). FERA is trained on a new dataset built to overcome the limitations of prior work. We next situate FERA within the context of related research on fencing action recognition and pose-based tracking, before detailing our dataset and methodology.

2. Related Work

2.1. AI in fencing

AI has been explored in fencing, but existing approaches face notable limitations. FenceNet and related models report over 85% accuracy on the Fencing Footwork Dataset [14, 25], which contains 652 videos from 10 fencers annotated with actions such as step forward, step backward, rapid lunge, incremental-speed lunge, lunge with waiting, and jumping-sliding lunge. While valuable for modeling footwork, the dataset is narrow: it omits many actions, particularly blade-related ones, that are essential for referee decisions in foil. All recordings come from a single environment with fixed, straight-on angles, limiting robustness in real-world conditions. Each video shows only one fencer, without opponent exchanges. As a result, the clips represent best-case scenarios, lacking the reflexive responses and corrections that occur in actual bouts.

Although such conditions simplify training and yield high reported accuracy, models trained on this data cannot generalize to full foil bouts with diverse speeds, movements, and camera perspectives. Our dataset and label-

ing protocol address these shortcomings, albeit at the cost of increased modeling difficulty. To meet this challenge, FERA builds on pose-based analysis and robust multi-person tracking to extract reliable motion cues in real bouts.

2.2. Pose Estimation and Tracking

Human pose estimation is central to analyzing athletic performance because it converts raw video into structured joint representations, reducing noise. While direct video preprocessing can yield results, pose estimation has proven more effective for extracting relevant motion information. Early work, such as OpenPose, introduced Part Affinity Fields to detect body parts and associate them with individuals in crowded scenes [4], enabling multi-person keypoints and downstream sport applications. Later top-down approaches improved accuracy by cropping per-person bounding boxes before extraction [22]. More recently, vision transformers (e.g., ViTPose) have advanced accuracy further through large-scale pretraining and attention [23]. In this work, we use MMPose [15], which provides multiple pose-extraction frameworks. Specifically, FERA utilizes RTMPose [9] for pose estimation and RTMDet [13] for bounding box detection. RTMPose is lightweight, real-time, and maintains competitive accuracy.

Accurate per-frame keypoints are only part of the solution. Tracking identities and poses over time, especially under occlusion from referees, spectators, or when fencers cross paths, is challenging. Multi-object trackers such as DeepSORT [20] link detections using motion cues and can re-connect after short occlusions. Newer trackers like ByteTrack [24] retain all detections, including low-confidence ones, to avoid losing objects during fast, blurry frames. FERA instead employs a custom tracker tailored for fencing, combining a distance function with Norfair [18, 19].

A further challenge is reliably detecting the fencers themselves. No fencing-specific detector currently exists to distinguish the two active fencers from referees or spectators. Prior work assumes either single-subject lab recordings or generic multi-person tracking, which cannot guarantee correct selection. Ignoring this issue undermines the pipeline: the chance of selecting the wrong subject among many is high. Even filtering for the most confident poses often selects the referee, who is more static, rather than the fencer performing a fast action.

3. Data

To overcome the limitations of prior single-fencer, single-angle datasets, we constructed a dataset of fencing bout clips designed to capture two-fencer exchanges under varied camera angles. The dataset is derived from professional match videos (720p, 25 fps) from three Grand Prix competitions involving approximately 130 competitors. Each match video is segmented into the final seven seconds pre-

ceding a touch. Referee decisions are inferred by analyzing the score: if the score changes before another touch occurs, a point is awarded. By aligning these score changes with detected hit events and applying the rules, we obtain referee decisions associated with the clips. This process yields a large set of segments paired with referee outcomes, which form the basis of the rule-reasoning dataset. Each clip is then manually annotated frame by frame to identify the moves performed, providing the data required for FERA-MDT. Details of hit detection, score extraction, and label assignment are given in Section 3.1.

3.1. Dataset specifics and labeling

Many fencing videos display static overlays for scoring and hit lights. We manually locate the coordinates where the hit lights appear and the score digits are shown. In these regions, reference images are compared to video frames; if the color similarity exceeds tuned thresholds, a hit is detected. For score extraction, number recognition is applied to the identified score zones.

With clips and touch times determined, actions are annotated frame by frame using a custom graphical interface (Figure 1). Each clip is segmented into moves and labeled with one or more of the following actions: step forward, step backward, half step forward, half step backward, lunge, flèche, wait, parry, beat, counterattack, fake, and hit. Each segment is also assigned a blade position from {4, 6, 7, 8, other}. In cases where moves overlap (e.g., beat + step forward), the interval is marked by the endpoints of the longer action, and both labels are retained.

Note to fencers: the *hit* label may appear arbitrary, but it is simple: it indicates the fencer extended their arm with the intention to score. It does not guarantee that contact was successful.



Figure 1. Custom graphical labeler used to annotate moves and blade positions frame by frame.

In Figure 1, the fencer poses are already visualized in the video. This is done so that, in case the fencer selector fails and chooses an incorrect person, we omit the entire clip to prevent introducing incorrect data.

3.2. Data Distribution

In total, the dataset contains 1,734 videos, covering 2,386 move instances, with an average of 1.38 moves per video. The moves are skewed, with the most common actions being step forward (28.8%), hit (19.9%), and step backward (14.6%), while rare moves such as flèche account for less than 1% (Table 1a).

Table 1. Dataset distributions for moves and blade positions.

(a) Moves			(b) Blade positions		
Move	Count	%	Blade position	Count	%
Step forward (1)	687	28.8	6	1114	64.2
Step backward (2)	349	14.6	8	410	23.6
Half step forward (3)	127	5.3	7	95	5.5
Half step backward (4)	87	3.6	4	85	4.9
Lunge (5)	232	9.7	Other	30	1.7
Flèche (6)	11	0.5			
Wait (7)	71	3.0			
Parry (8)	72	3.0			
Beat (9)	150	6.3			
Counterattack (10)	77	3.2			
Fake (11)	49	2.1			
Hit (12)	474	19.9			

Blade positions are highly imbalanced: position 6 accounts for 64.2% of annotations, followed by position 8 (23.6%), while positions 4, 7, and other together represent only 12.2% (Table 1b). This skew is difficult to mitigate, since fencers typically favor one or two blade positions that they switch between during a match. As most competitors rely on positions 6 and 8 far more than 4 or 7, instances combining a rare move with a rare blade position are exceedingly uncommon.

Data ethics and usage. All videos used in this study are publicly available on YouTube. The dataset is used strictly for academic research under fair use and is not intended for commercial purposes. All annotations were created manually by fencing experts. Because no direct human subjects were involved, informed consent was not required. All released data are fully anonymized.

4. Methodology

4.1. FERA pipeline overview

The FERA pipeline converts raw video into structured referee decisions through four stages: (i) pose estimation, (ii) feature engineering, (iii) Transformer-based move and blade detection (FERA-MDT), and (iv) language-model reasoning (FERA-LM). This overview follows that flow and introduces the dynamic windowing mechanism used to determine which frames are passed to FERA-MDT.

FERA begins by extracting 2D skeleton poses from video, which are then normalized and augmented with the kinematic features described in Section 4.3. Frame sequences are next fed into FERA-MDT and evaluated for

detection confidence. If confidence is insufficient, the window expands incrementally by one frame, up to a maximum of forty. If the limit is reached without a confident detection, the starting frame shifts forward, and the process repeats. FERA continues until a confident detection is made. For half-steps, the system checks for a subsequent full step before finalizing the label. This dynamic window accommodates a wide variation in move length; static windows tend to overlap actions and create boundary errors. Once all moves are identified, the predicted actions and blade positions for both fencers are combined with encoded priority rules and passed to FERA-LM, which produces a concise decision and explanation. The following sections describe each stage in detail, beginning with fencer selection and tracking.

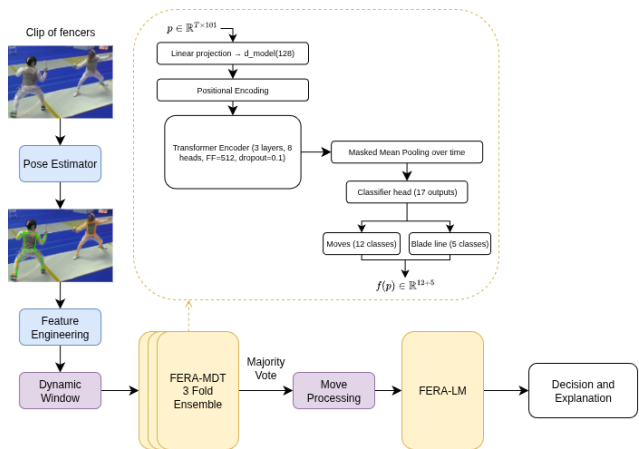


Figure 2. Pipeline visualization.

4.2. Pose Estimation

The first stage of FERA requires accurately identifying the two active fencers and tracking their skeletons across frames, even under occlusion. This process consists of three components: fencer filtering, tracking, and joint extraction.

Fencer filtering. At the start of each clip, a grace period is used to search for candidate fencers. Candidates must occupy at least 3% of the frame area, exceed a confidence threshold (> 0.20), and not touch the bottom edge (referees are often visible only from the torso upward). Each candidate is then scored with a criterion tuned to select fencers, prioritizing size and penalizing positions that are too high or low in frame.

Tracking. Tracking is implemented using Norfair and a custom distance function that combines intersection-over-union (IoU) and centroid distance [18, 19]. If an ID is lost, the system attempts to reassign it by matching new detections to the last known bounding box via IoU overlap.

Pose similarity scoring further prevents switches to background individuals. A light exponential moving average (EMA) smooths the joint trajectories, retaining valid positions when detections are missing and reducing jitter.

Pose extraction. Bounding boxes and skeletons are obtained using MMDetection and MMPose [5, 15]. Specifically, we employ `rtmpose-m_8xb256-420e_coco-256x192` for pose extraction and `rtmdet_tiny_8xb32-300e_coco` for detection, selected as the fastest available models within RTMPose [9] and RTMDet [13] while maintaining competitive accuracy.

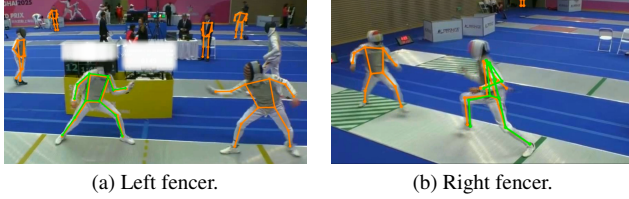


Figure 3. Pose candidate visualizations for both fencers. Selected fencers are highlighted in green.

4.3. Feature Engineering

The second stage of FERA involves feature engineering. While raw joints are informative, engineered features capture temporal and geometric dynamics that joints alone cannot convey.

After stage one, 17 joints are available. Because head joints are unreliable due to masks, we discard five of them, leaving 12 body joints. To remove background dependence, we compute a scale- and translation-invariant representation by centering each frame at the pelvis and normalizing by average torso length:

$$\tilde{\mathbf{p}}_{i,t} = \frac{\mathbf{p}_{i,t} - \frac{1}{2}(\mathbf{P}_{Lhip,t} + \mathbf{P}_{Rhip,t})}{\frac{1}{2}(\|\mathbf{P}_{Lsh,t} - \mathbf{P}_{Lhip,t}\| + \|\mathbf{P}_{Rsh,t} - \mathbf{P}_{Rhip,t}\|)},$$

where $\mathbf{p}_{i,t} \in \mathbb{R}^2$ is the (x, y) position of joint i at frame t .

From these normalized joints, we derive additional features:

Pairwise distances:

$$d_{ab,t} = \|\tilde{\mathbf{p}}_{a,t} - \tilde{\mathbf{p}}_{b,t}\|,$$

for key pairs such as hand-to-hand, foot-to-foot, and shoulder/hip widths.

Joint angles: at elbows and knees. For three joints a - b - c ,

$$\theta_{abc,t} = \arccos \frac{(\tilde{\mathbf{p}}_{a,t} - \tilde{\mathbf{p}}_{b,t}) \cdot (\tilde{\mathbf{p}}_{c,t} - \tilde{\mathbf{p}}_{b,t})}{\|\tilde{\mathbf{p}}_{a,t} - \tilde{\mathbf{p}}_{b,t}\| \|\tilde{\mathbf{p}}_{c,t} - \tilde{\mathbf{p}}_{b,t}\|}.$$

Torso orientation: represented as sin and cos of the angle between shoulder and hip centers.

Arm extension: magnitude and normalized direction of shoulder-wrist vectors.

Center of mass (CoM): average of all valid joints.

To capture dynamics, temporal derivatives are also included:

$$\mathbf{v}_{i,t} = \tilde{\mathbf{p}}_{i,t} - \tilde{\mathbf{p}}_{i,t-1}, \quad \mathbf{a}_{i,t} = \mathbf{v}_{i,t} - \mathbf{v}_{i,t-1},$$

for all normalized joints and the CoM.

Altogether, each frame is represented by a 101-dimensional vector: 24 joint coordinates, 2 CoM features, 11 distances, 4 angles, 2 torso orientation features, 6 arm-extension features, 24 velocities, 24 accelerations, and 4 CoM velocity/acceleration features. These descriptors serve as the input tokens to FERA-MDT.

4.4. FERA-MDT

The core of FERA is FERA-MDT, an encoder-only Transformer for multi-label move and blade recognition. We describe its architecture, loss functions, training, augmentation, and hyperparameter tuning.

Architecture. Each input frame has 101 features (Sec. 4.3), projected to a 128-dimensional embedding. The model comprises three encoder layers, each with eight attention heads and a feed-forward dimension of 512, with dropout of 0.1. Temporal aggregation uses masked mean pooling to ensure consistent handling of variable-length sequences.

Positional encoding and attention. Temporal structure is preserved through sinusoidal encodings with dropout:

$$\begin{aligned} PE_{(pos,2i)} &= \sin\left(\frac{pos}{10000^{2i/d}}\right), \\ PE_{(pos,2i+1)} &= \cos\left(\frac{pos}{10000^{2i/d}}\right). \end{aligned} \quad (1)$$

Multi-head self-attention is applied as

$$\text{Attention}(Q, K, V) = \text{softmax}\left(\frac{QK^\top}{\sqrt{d_k}} + M\right)V,$$

with key-padding mask M to exclude padded tokens.

Output and loss functions. The final layer is a linear classifier ($128 \rightarrow 17$). The first 12 outputs correspond to moves (multi-label, weighted binary cross-entropy), and the last 5 to blade positions (single-label, softmax cross-entropy). Move loss is

$$\begin{aligned} L_{\text{move}} &= -\frac{1}{N} \sum_i w_i \left[y_i \log \sigma(z_i) \right. \\ &\quad \left. + (1 - y_i) \log (1 - \sigma(z_i)) \right], \end{aligned} \quad (2)$$

with weights w_i from inverse class frequency. Blade loss is

$$L_{\text{blade}} = - \sum_{c=1}^5 y_c \log \text{softmax}(z)_c.$$

The combined loss is

$$L = L_{\text{move}} + 0.677 L_{\text{blade}},$$

where the blade weight (0.677) was selected via Optuna to balance gradients and label counts.

Training configuration. Training uses AdamW [12] with learning rate 10^{-3} , weight decay 10^{-4} , and betas (0.9, 0.999). The schedule is 3-epoch warmup, 5-epoch flat, then cosine annealing [11]. Gradients are clipped at $\|g\|_2 \leq 0.5$; batch size is 24. Evaluation uses 5-fold cross-validation with an 80/10/10 split. All experiments are implemented in PyTorch [16].

Data augmentation and balancing. To improve robustness, augmentation is applied after the data is split. Methods include temporal jitter ($\Delta t \sim \{-2, \dots, 2\}$), Gaussian noise ($\epsilon \sim \mathcal{N}(0, 0.05^2)$), rotational noise ($\theta \sim U(-0.05, 0.05)$), and scaling ($s \sim U(0.95, 1.05)$). To mitigate imbalance, minority moves are oversampled up to 400 per class, and the majority blade class “6” is downsampled to two-thirds of the others.

Hyperparameter selection. Hyperparameters were tuned with Optuna [1]. Across 300 trials, we explored model size, loss weighting, weight decay, and other settings. The top 10 runs were analyzed for recurring patterns, and their best-performing elements were combined into the final model.

4.5. FERA-LM

After generating move and blade predictions, FERA requires reasoning with priority rules to produce valid and explainable decisions. To address this, we introduce FERA-LM, the fourth stage of the pipeline. FERA-LM is a compact distilled language model.

Using DeepSeek-R1-Distill-Qwen-14B as the teacher model (the largest model we could run), we generated referee decisions with a structured prompt [6].

Prompt engineering for the language model.

I am an expert fencing referee. Based solely on the fencing moves and rules provided below, I will determine the correct decision. I will provide my answer in two parts as follows:

Decision: Exactly one line saying whether left or right should have priority at the end of the clip, or none

Explanation: I will provide a concise explanation of why I reached the decision in part 1, referencing moves and rules relevant to the given moves below.

I also will not include any additional commentary, train of thought text, or anything else irrelevant to the concise explanation beyond these two parts.

I will not reference rules that are not invoked in the move sequences.

At the very end of my entire answer, I will output !!! on its own line, indicating I have finished.

Rules: (Through a FAISS index [10], we pull the relevant rules from my generated index file to insert here)

Left Fencer: (moves)

Right Fencer: (moves)

My expert Referee Decision and explanation:

This prompt enforces a strict two-part response, enabling straightforward post-processing. Responses are capped at 150 tokens to ensure conciseness, and generation is forced to be deterministic for consistent outputs [21].

The distilled student model is DistilGPT-2, trained with Causal Language Modeling on data produced by the teacher. This yields a far less computationally intensive model while retaining decision quality [8]. At present, FERA-LM remains in an early stage, as its accuracy depends heavily on FERA-MDT. Future iterations will revisit distillation once move detection achieves higher F1 scores.

5. Results

We evaluate FERA in two ways: (i) an end-to-end case study demonstrating how the full pipeline produces referee decisions, and (ii) quantitative comparisons of FERA-MDT with baseline models, supplemented by ablation studies.

5.1. End-to-end Example

We first present an example clip where the referee ruled that the left fencer held priority. The prompt template is given in Section 4.5. In this case, FERA-MDT correctly identifies the actions performed by both fencers, and FERA-LM produces a concise decision and explanation that aligns with the referee’s judgment.

Rules.

If an attack is initiated but falls short or misses, priority shifts to the other fencer.

Priority is given to the fencer who initiates the attack unless it is interrupted.

Fencing moves:

Left: [80–112] step forward (blade pos. 8); [112–134] step forward + beat (blade pos. 8); [134–146] lunge + hit (blade pos. 6).

Right: [83–110] step backward (blade pos. 6); [110–138] fake (blade pos. 6); [138–148] counterattack + hit (blade pos. 6).



(a) Left fencer step forward + beat, right fencer stepping back. (b) Left fencer lunging, right fencer counterattacking.

Figure 4. Illustrative frames from the bout corresponding to the described moves.

Model Output.

Decision: Left

Explanation: The left fencer initiated an attack with a step forward since the right fencer stepped backward. The left fencer then attacks with a lunge, hit (134–146) and the right fencer responds with counterattack, hit (138–148). According to the rules, the priority never shifts to the right fencer.

!!!

5.2. Evaluation metrics.

We now move from a representative clip to aggregate performance. We report four classification metrics and three calibration metrics.

Classification.

- Macro-F1 = $\frac{1}{C} \sum_c F1_c$: treats all classes equally, so rare moves (e.g., *flèche*) contribute as much as common ones.
- Weighted-F1 = $\sum_c \frac{n_c}{\sum_j n_j} F1_c$: weights each class by frequency, downplaying errors on infrequent moves.
- Micro-F1 = $\frac{2 \sum_c TP_c}{2 \sum_c TP_c + \sum_c FP_c + \sum_c FN_c}$: overall accuracy across all moves, dominated by frequent classes.
- Hamming loss = $\frac{1}{NC} \sum_{i=1}^N \sum_{c=1}^C \mathbf{1}[y_{i,c} \neq \hat{y}_{i,c}]$: fraction of misclassified labels (false positives + false negatives); lower is better.

For each class c , precision, recall, and F1-score are:

$$P_c = \frac{TP_c}{TP_c + FP_c}, \quad R_c = \frac{TP_c}{TP_c + FN_c}, \quad F1_c = \frac{2P_c R_c}{P_c + R_c}.$$

Calibration.

$$ECE = \sum_{m=1}^M \frac{|B_m|}{N} |\text{acc}(B_m) - \text{conf}(B_m)|,$$

$$MCE = \max_m |\text{acc}(B_m) - \text{conf}(B_m)|,$$

$$\text{Brier} = \frac{1}{NC} \sum_{i=1}^N \sum_{c=1}^C (y_{i,c} - \hat{p}_{i,c})^2.$$

ECE summarizes average calibration quality; MCE highlights worst-case miscalibration; Brier combines calibration and sharpness into a single probability-quality measure.

5.3. Move detection model comparisons

We compare FERA-MDT against three baseline architectures: a simple Transformer encoder, a BiLSTM, and a Temporal CNN (TCN).

As shown in Table 2, FERA-MDT consistently outperforms all baselines on Macro-F1 and Hamming loss, indicating stronger performance on both common and rare fencing moves. The BiLSTM performs closest to FERA-MDT, as recurrent architectures capture short-term motion dependencies well. However, given the complex multi-label structure and long-range dependencies in our setting, FERA-MDT handles them more effectively. The baseline Transformer lags due to weak regularization and lack of effective pooling, whereas FERA-MDT benefits from dropout-stabilized sinusoidal encodings, masked mean pooling, and a structured encoder stack. The TCN achieves the highest Weighted-F1, reflecting a bias toward dominant classes such as step forward and hit. For refereeing, this is undesirable since accurate recognition of rare actions is equally important.

Table 3 shows calibration results. Both the BiLSTM and baseline Transformer perform substantially worse than FERA-MDT and the TCN. Between the latter two, the TCN achieves lower ECE and MCE but a higher Hamming loss than FERA-MDT. This suggests that its apparently better calibration stems from overspecialization on frequent classes, while FERA-MDT balances rare- and common-class predictions more effectively.

Overall, FERA-MDT achieves high accuracy, robust rare-class recognition, and reasonable calibration, making it the strongest candidate for referee assistance.

Model	Macro-F1 ↑	Micro-F1 ↑	Weighted-F1 ↑	Hamming ↓
FERA-MDT	0.549	0.543	0.558	0.158
BiLSTM [17]	0.537	0.531	0.550	0.166
Baseline Transformer	0.533	0.524	0.546	0.170
Temporal CNN (TCN) [2]	0.520	0.519	0.569	0.184

Table 2. Classification performance averaged across 5 folds.

Model	ECE ↓	MCE ↓	Brier ↓
FERA-MDT	0.152	0.458	0.135
BiLSTM	0.187	0.512	0.146
Baseline Transformer	0.191	0.498	0.143
Temporal CNN (TCN)	0.110	0.446	0.140

Table 3. Calibration metrics averaged across 5 folds.

5.4. Co-occurrence Analysis

Because referee decisions depend on combinations of actions, we assess whether models reproduce the ground-truth co-occurrence structure. Figures 5–8 compare co-occurrence mappings across architectures. The left matrix shows ground-truth labels, while the right shows model predictions; the closer the two, the better the model captures true co-occurrences. FERA-MDT produces mappings that

most closely mirror the ground-truth distribution, whereas baselines tend to over-activate frequent moves and under-represent rarer ones.

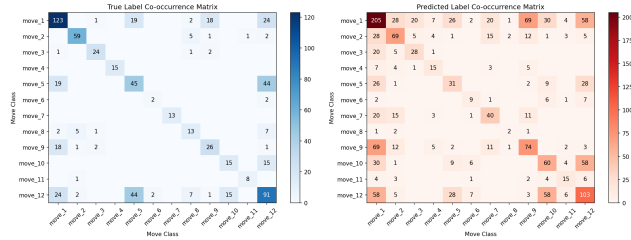


Figure 5. Co-occurrence mapping (Fold 5) for FERA-MDT.

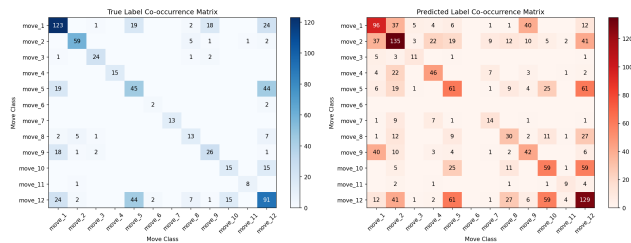


Figure 6. Co-occurrence mapping (Fold 5) for BiLSTM.

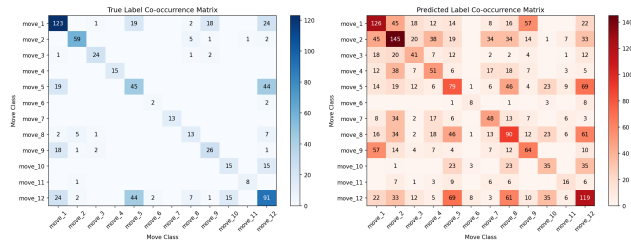


Figure 7. Co-occurrence mapping (Fold 5) for the baseline Transformer.

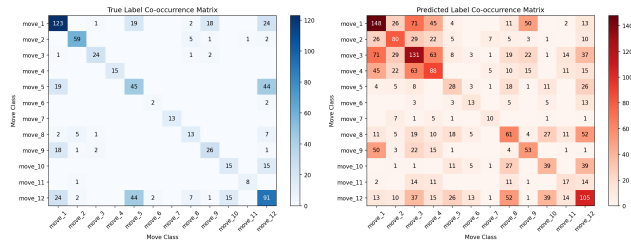


Figure 8. Co-occurrence mapping (Fold 5) for the Temporal CNN (TCN).

These results confirm that FERA-MDT captures not only individual moves but also their distributions and interactions. We next analyze which design choices contribute most to this performance.

5.5. Ablations

To identify which components contribute most to performance, we performed ablations on FERA-MDT while keeping all other settings fixed (baselines were not ablated). We report both classification (average Macro-F1 across five folds) and calibration metrics (average ECE, MCE, and Brier score [3, 7]).

Table 4 summarizes the results. The full FERA-MDT configuration achieves the highest Macro-F1 (0.549) while maintaining strong calibration (ECE = 0.152, MCE = 0.458, Brier = 0.135). Removing per-class thresholds reduces Macro-F1 to 0.511, confirming that threshold tuning is critical. Using only the 12 normalized joints (24D) yields a Macro-F1 score of 0.534, showing that engineered features improve performance but are not solely responsible. Notably, calibration worsens substantially in the raw-joints ablation, indicating that features primarily enhance reliability with secondary accuracy gains.

Augmentation strategies provide complementary benefits. Individually, noise-only, temporal-only, and feature-specific augmentations yield Macro-F1 scores of 0.542, 0.525, and 0.537, respectively. Combining all strategies produces the best robustness and the top score (0.549). Figures 9 and 10 illustrate the instability of single augmentation: in Fold 2, the model collapses to frequent moves, while in Fold 3, it nearly matches the full model. Despite occasional strong folds, the average remains lower (0.537), underscoring the need for combined augmentation and calibration to stabilize performance.

Finally, per-class temperature scaling improves calibration without changing F1, and down-weighting blade loss slightly benefits both calibration and classification.

Overall, these ablations emphasize that FERA-MDT’s complete design—feature engineering, diverse augmentation, calibrated thresholds, and tailored loss weighting—is necessary to achieve both strong classification and reliable confidence estimates.

Variant	Macro-F1 ↑	ECE ↓	MCE ↓	Brier ↓
All Features	0.549	0.152	0.458	0.135
No per-class thresholds	0.511	0.140	0.460	0.137
Raw joints (24D, no features)	0.534	0.184	0.515	0.149
Noise-only augmentation	0.542	0.175	0.467	0.141
Temporal augmentation only	0.525	0.200	0.535	0.164
Feature-specific augmentation only	0.537	0.154	0.487	0.144
No augmentation	0.541	0.176	0.545	0.150
No per-class temperature scaling	0.549	0.178	0.493	0.142
Equal loss weights (move = blade)	0.544	0.179	0.499	0.146

Table 4. Ablations: Macro-F1 and calibration metrics (average over 5 folds).

These factors improve both accuracy and reliability, but also highlight where the system remains data- and sensing-

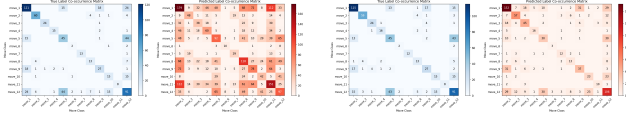


Figure 9. Feature-specific augmentation only (Fold 2, poor performance).

Figure 10. Feature-specific augmentation only (Fold 3, strong performance).

limited, which we address next.

6. Limitations and Future Work

Our study faces several limitations, many of which suggest clear directions for future work. The primary constraint is data. With no publicly available datasets containing extensive move annotations, we relied on manual labeling, which limited model accuracy. Nevertheless, performance improved steadily as the dataset grew: with $\sim 1,000$ annotated segments, F1 plateaued near 0.40, while doubling to 2,000 segments raised F1 to 0.549. This trend suggests that long-tail actions remain a bottleneck, and that expanding the dataset—especially for rare moves—will further improve accuracy.

Another limitation is that FERA relies on publicly available pose detectors, which do not support blade detection. Developing a blade-specific extractor would enable FERA-MDT to incorporate precise blade positions, thereby increasing the reliability of contact detection. At the reasoning stage, FERA-LM depends on the outputs of FERA-MDT, meaning that motion recognition errors introduce noise during both teacher generation and student distillation. Improvements in move detection should reduce this noise, leading to more accurate language-model decisions.

Generalization also remains a challenge. Our dataset consists exclusively of professional fencers, often recorded from elevated camera angles, which limits adaptability to beginners and to more varied viewpoints. Future work may incorporate 3D joint extraction to mitigate camera-angle sensitivity and extend testing to broader fencer populations.

Finally, we did not employ athlete-disjoint splits for training and validation, as we lack metadata to link clips to individual fencers. While this is partially mitigated by scale—our dataset spans roughly 130 competitors—the risk of overfitting to individuals cannot be ruled out.

Overall, these limitations outline a roadmap: larger and more diverse datasets, explicit blade detection, improved distillation from cleaner labels, and greater attention to generalization. Addressing these factors will enable both more dependable referee assistance and broader coaching applications.

7. Conclusion

We conclude by first emphasizing the motivation for developing FERA. In modern-day foil fencing, refereeing is entirely manual, with the only automated aspect being the lights, which display who hit whom. No existing automated systems have been made to assist or validate human decisions. Prior work on fencing move recognition has been limited to small subsets of footwork actions and often uses specialized sensors for extra data. Therefore, our goal was to design the first prototype referee system that operates directly from monocular video, allowing practical deployment in everyday training settings. To that end, we present (i) the first prototype AI referee for foil fencing, (ii) a new dataset with annotated moves and blade positions, and (iii) a combined pipeline that integrates pose-based recognition with rule-grounded reasoning. While FERA-MDT’s current performance (F1 = 0.549) highlights the challenge of this subject, our results demonstrate the feasibility of utilizing Transformer-based motion understanding to extract and detect actions performed by fencers under real-world scenarios. FERA could also be extended beyond refereeing. By aggregating recognized actions and blade positions, the system could recognize patterns and offer data-driven feedback to athletes and coaches. We hope this work inspires further exploration in AI-driven sports analytics.

References

- [1] Takuya Akiba, Shotaro Sano, Toshihiko Yanase, Takeru Ohta, and Masanori Koyama. Optuna: A next-generation hyperparameter optimization framework. In *Proceedings of the 25th ACM SIGKDD International Conference on Knowledge Discovery & Data Mining*, page 2623–2631, New York, NY, USA, 2019. Association for Computing Machinery.
- [2] Shaojie Bai, J. Zico Kolter, and Vladlen Koltun. An empirical evaluation of generic convolutional and recurrent networks for sequence modeling, 2018.
- [3] Glenn W. Brier. Verification of forecasts expressed in terms of probability. *Monthly Weather Review*, 78(1):1–3, 1950.
- [4] Zhe Cao, Gines Hidalgo, Tomas Simon, Shih-En Wei, and Yaser Sheikh. Openpose: Realtime multi-person 2d pose estimation using part affinity fields. *IEEE Transactions on Pattern Analysis and Machine Intelligence*, 43(1):172–186, 2021.
- [5] Kai Chen, Jiaqi Wang, Jiangmiao Pang, Yuhang Cao, Yu Xiong, Xiaoxiao Li, Shuyang Sun, Wansen Feng, Ziwei Liu, Jiarui Xu, et al. Mmdetection: Open MMLab detection toolbox and benchmark. *arXiv preprint arXiv:1906.07155*, 2019.
- [6] DeepSeek-AI. Deepseek-r1-distill-qwen-14b (model card). <https://huggingface.co/deepseek-ai/DeepSeek-R1-Distill-Qwen-14B>, 2025. accessed: 2025-09-08.
- [7] Chuan Guo, Geoff Pleiss, Yu Sun, and Kilian Q. Weinberger. On calibration of modern neural networks. In *Proceedings*

- of the 34th International Conference on Machine Learning, pages 1321–1330. PMLR, 2017.
- [8] Hugging Face. Distilgpt-2 (model card). <https://huggingface.co/distilbert/distilgpt2>, 2024. accessed: 2025-09-08.
- [9] Tao Jiang, Peng Lu, Li Zhang, Ningsheng Ma, Rui Han, Chengqi Lyu, Yining Li, and Kai Chen. Rtmpose: Real-time multi-person pose estimation based on mmpose, 2023.
- [10] Jeff Johnson, Matthijs Douze, and Hervé Jégou. Billion-scale similarity search with gpus. *IEEE Transactions on Big Data*, 7(3):535–547, 2021.
- [11] Ilya Loshchilov and Frank Hutter. SGDR: Stochastic gradient descent with warm restarts. In *International Conference on Learning Representations*, 2017.
- [12] Ilya Loshchilov and Frank Hutter. Decoupled weight decay regularization. In *International Conference on Learning Representations*, 2019.
- [13] Chengqi Lyu, Wenwei Zhang, Haian Huang, Yue Zhou, Yudong Wang, Yanyi Liu, Shilong Zhang, and Kai Chen. Rtmddet: An empirical study of designing real-time object detectors, 2022.
- [14] Filip Malawski. Fencing footwork dataset (ffd). <https://home.agh.edu.pl/~fmal/ffd/>, 2016. accessed: 2025-09-08.
- [15] OpenMMLab. Mmpose: OpenMMLab pose estimation toolbox and benchmark. <https://github.com/open-mmlab/mmpose>, 2024. accessed: 2025-09-08.
- [16] Adam Paszke, Sam Gross, Francisco Massa, Adam Lerer, James Bradbury, Gregory Chanan, Trevor Killeen, Zeming Lin, Natalia Gimelshein, Luca Antiga, et al. PyTorch: An imperative style, high-performance deep learning library. In *Advances in Neural Information Processing Systems (NeurIPS)*, 2019.
- [17] M. Schuster and K.K. Paliwal. Bidirectional recurrent neural networks. *IEEE Transactions on Signal Processing*, 45(11):2673–2681, 1997.
- [18] TryoLabs. Norfair documentation. <https://tryolabs.github.io/norfair/2.2/reference/>, 2023. accessed: 2025-09-08.
- [19] TryoLabs. Norfair: Lightweight python library for real-time multi-object tracking. <https://github.com/tryolabs/norfair>, 2023. accessed: 2025-09-08.
- [20] Nicolai Wojke, Alex Bewley, and Dietrich Paulus. Simple online and realtime tracking with a deep association metric. In *2017 IEEE International Conference on Image Processing (ICIP)*, pages 3645–3649, 2017.
- [21] Thomas Wolf, Lysandre Debut, Victor Sanh, Julien Chaumond, Clément Delangue, Anthony Moi, Pierric Cistac, Tim Rault, Rémi Louf, Morgan Funtowicz, et al. Transformers: State-of-the-art natural language processing. In *Proceedings of the 2020 Conference on Empirical Methods in Natural Language Processing: System Demonstrations (EMNLP Demos)*, pages 38–45, 2020.
- [22] Bin Xiao, Haiping Wu, and Yichen Wei. Simple baselines for human pose estimation and tracking. In *Proceedings of the European Conference on Computer Vision (ECCV)*, pages 466–481, 2018.
- [23] Yufei Xu, Jing Zhang, Qiming Zhang, and Dacheng Tao. Vit-pose: Simple vision transformer baselines for human pose estimation, 2022.
- [24] Yifu Zhang, Peng Sun, Yi Jiang, Dongdong Yu, Xinze Weng, Zhaoqi Yuan, Ping Luo, Wen Liu, and Xiaogang Wang. ByteTrack: Multi-object tracking by associating every detection box. In *Proceedings of the European Conference on Computer Vision (ECCV)*, 2022.
- [25] Kevin Zhu, Alexander Wong, and John McPhee. Fencenet: Fine-grained footwork recognition in fencing. In *CVPR Workshops*, 2022.